Distribution Agreement

In presenting this thesis as a partial fulfillment of the requirements for a degree from Emory University, I hereby grant to Emory University and its agents the non-exclusive license to archive, make accessible, and display my thesis in whole or in part in all forms of media, now or hereafter now, including display on the World Wide Web. I understand that I may select some access restrictions as part of the online submission of this thesis. I retain all ownership rights to the copyright of the thesis. I also retain the right to use in future works (such as articles or books) all or part of this thesis.

Anshuman Swain   April 13, 2021

High-Resolution Magic-Angle Spinning and Nuclear Magnetic Resonance Relaxometry
Investigations of Tendon

by

Anshuman Swain

David Reiter

Adviser

Department of Chemistry

David Reiter

Adviser

Candace C. Fleischer

Committee Member

John Heemstra

Committee Member

2021

High-Resolution Magic-Angle Spinning and Nuclear Magnetic Resonance Relaxometry
Investigations of Tendon

By

Anshuman Swain

David Reiter

Adviser

An abstract of
a thesis submitted to the Faculty of Emory College of Arts and Sciences
of Emory University in partial fulfillment
of the requirements of the degree of
Bachelor of Science with Honors

Department of Chemistry

2021

Abstract

High-Resolution Magic-Angle Spinning and Nuclear Magnetic Resonance Relaxometry
Investigations of Tendon

By Anshuman Swain

Tendons are an important load-bearing tissue in the musculoskeletal system, with a
matrix composition closely associated with its functional status. The extracellular matrix of
tendon is composed of collagen fibrils and non-collagenous components consisting of
proteoglycans, lipids, and metabolites. Recent work using ultrashort echo time magnetic
resonance imaging (UTE-MRI) has reported chemical shifts consistent with proteoglycan and
lipid chemical groups. However, there is a lack of prior nuclear magnetic resonance (NMR)
studies available to interpret these signals. High-resolution magic-angle spinning (HR-MAS)
NMR and NMR relaxometry are used to determine the origin of the chemical shifts and biases in
the estimates of relaxation measurements from UTE imaging. This study uses one-dimensional
and two-dimensional HR-MAS NMR to characterize tendon matrix composition, providing a
clearer interpretation of *in vivo* UTE-MRI chemical shift signals and their relation to tendon
matrix integrity. This study also utilizes NMR relaxometry to explore water dynamics in tendon,
allowing for a better interpretation of relaxation signals acquired from UTE-MRI. Five ex vivo
samples of both ovine Achilles and rat rotator cuff tendon are obtained. A Bruker Avance III
spectrometer at 400 MHz is used to acquire data and MATLAB (MathWorks, USA) and
Mestrenova (Mestrelabs, Spain) are used to process and analyze data. Peak assignments are
made using prior literature and the HMDB. Analysis of the spectra obtained from HR-MAS
NMR shows peaks attributed to biomolecules and residues comprising collagen fibrils and non-
collagenous matrix components, allowing for the determination of the origin of chemical shift
signals in UTE-MRI. Analysis of the spectra obtained from NMR relaxometry shows two
distinct pools of water in tendon that are in chemical exchange, providing a clearer interpretation
of relaxation measurements from UTE-MRI. It is concluded that both methods help to better
interpret chemical shift and relaxation signals obtained from UTE-MRI of tendon.

High-Resolution Magic-Angle Spinning Nuclear Magnetic Resonance Investigations of Tendon
Composition and Function

By

Anshuman Swain

David Reiter

Adviser

A thesis submitted to the Faculty of Emory College of Arts and Sciences
of Emory University in partial fulfillment
of the requirements of the degree of
Bachelor of Science with Honors

Department of Chemistry

2021

Acknowledgements

I would like to acknowledge Muhammad Ali Raza Anjum and Jingting Becky Yao, two fantastic postdoctoral fellows who I had the pleasure of working with and contributing enormously to my project and serving as members on my committee. I would like to acknowledge Dr. Johannes Leisen in the Department of Biochemistry and Chemistry at the Georgia Institute of Technology for helping tremendously in data collection. I would also like to acknowledge Dr. Johnna Temenoff and Dr. Joe Pearson for providing samples and aiding in sample handling.

Table of Contents

List of Figures

I.   Introduction

a.   Ultrashort echo time (UTE) imaging

Ultrashort echo time imaging is a valuable magnetic resonance imaging technique to image samples with short T_2 and T_2^* (transverse relaxation) times. Such samples consist of solid and semi-solid structures, including bone, tendon, and cartilage, with short relaxation times arising from magnetic susceptibility and anisotropic effects. UTE imaging is able to capture signal from rapidly decaying magnetization of a sample, producing images of compounds that would otherwise be undetectable using standard imaging sequences such as a spin-echo sequence (Fabich et al. 2014).

UTE imaging is implemented in tendon to observe signals from protons with relaxation times of ~0.1 to 10 ms, allowing for the characterization of the biophysical properties of the tissue compartments in tendon. Fitting a bi-exponential model to UTE decay data of tendon has been implemented due to the two observed relaxation components in tendon. The fast relaxing component of the bi-exponential model has been used to observe changes in composition and microstructure of tendon in patients with patellar tendinopathy (Kijowski et al. 2017). The slow relaxing component stems from the bulk water molecules surrounding the tendon collagen fibrils, while the fast relaxing component stems from water molecules bound to the interstitial space and side chains of collagen. Recently, Anjum et al. (2021) reported an oscillatory behavior in the decay data of tendon, obtained from UTE chemical shift imaging, facilitating the need to extend the current bi-exponential model of tendon. A multi-component model was fitted to the decay data that captures chemical shift information from the oscillations, obtaining two water relaxation components along with two off-resonance components to the water resonance frequency. The observed off-resonance frequencies were tentatively attributed to proteoglycans

3

and lipids based on known chemical shift groups attributed to these components and identification of these components in histological studies of tendon composition. Further studies need to be conducted in order to determine the origin of these off-resonance shifts and their potential for use as biomarkers. The relaxation components determined by the multi-component model, when compared to a standard bi-component model of tendon relaxation measurements, showed that the numerical fitting of the fast relaxing (short) component is influenced by the presence of off-resonance components and is thus underestimated in the bi-component model. As a result, further investigations must be made to assess the extent to which the short component can provide an accurate estimation of tendon microstructural and compositional changes in tendinopathy.

b. Objectives of the study

In this study, high resolution magic angle spinning (HR-MAS) nuclear magnetic resonance (NMR) spectroscopy is used on ex vivo samples of tendon from two different animal sources, specifically ovine Achilles tendon and rat rotator cuff tendon. Tendon is a semi-solid tissue with relaxation times on the order of less than 1 milliseconds. A standard ^{1}H NMR spectrum of tendon has broad peaks due to the anisotropic effects of dipolar coupling and magnetic susceptibility present in semi-solid tissues. By MAS, these broad peaks are significantly reduced by reducing dipolar coupling effects and chemical anisotropy, producing a better resolved spectrum. Using the spectra obtained from HR-MAS studies of tendon, the ability to make chemical shift assignments to the extracellular matrix (ECM) components is improved. Comparing the observed chemical shifts in HR-MAS of tendon to the chemical shift of the off-resonance components observed in UTE imaging will allow for the better assignment of the origin of these off-resonance components in UTE imaging. Consequently, the better assignment

of these off-resonance components observed in UTE imaging can lead to the development of potential biomarkers for assessing tendon structural integrity and tendinopathy.

In this study, 2D relaxometry, specifically T_2-store-T_2 experiments, is used to determine the molecular dynamics of water in tendon. Several models of tendon relaxation exist. Fullerton et al. (2007) describes a two compartment relaxation model of tendon involving a fast relaxing component and a slow relaxing component. The fast relaxing component stems from the primary hydration layer of rigid water molecules bound to the collagen molecule, while the slow relaxing component stems from the secondary hydration layer consisting of water molecules in exchange with water in the primary hydration layer. This study aims to identify exchange between the slow relaxing components and the fast relaxing components of tendon, in which protons in the interstitial space and those constituting the macromolecules exchange with the protons in collagen bulk water. Evaluating this exchange will better inform the multi-component fit of UTE imaging as exchange will affect the magnitude of the short and long relaxation components observed in tendon.

c. NMR Spectroscopy

Similar to other forms of spectroscopy, NMR spectroscopy arises from transitions of nuclei between two different energy states, specifically spin states (Kwan et al. 2011). Certain nuclei, such as ^1H and ^{13}C, have a magnetic dipole which can be visualized as small bar magnets. When a static magnetic field is imposed on these nuclei, they will seek to align in the direction of the magnetic field. Quantum mechanically, the nuclei have an angular momentum defined by the principles of quantum mechanics. Classically, the nuclei can be represented by spinning tops, so when a nucleus is placed in a magnetic field, it precesses about the magnetic field just as a top precesses when spun. The rate of precession is determined by a value known as the gyromagnetic

ratio, which is intrinsic to each type of nucleus. This rate of precession is described by the Larmor equation as follows:

$$\omega = \gamma B$$

where ω is the Larmor frequency in MHz, γ is the gyromagnetic ratio in MHz/Tesla, and B is the static magnetic field strength in Tesla. Nuclei in different chemical environments resonate at different frequencies due to electron shielding effects, changing the local magnetic field of the nuclei and resulting in a change in the static magnetic field strength as defined in the Larmor equation.

A change in energy state occurs when a radiofrequency pulse is applied perpendicular to the static magnetic field. This radiofrequency pulse is applied at the same frequency as the Larmor frequency, causing the net magnetization vector of nuclei to oriented itself in the transverse plane, orthogonal to the static magnetic field. The transverse relaxation of nuclei due to the loss of magnetization coherence, resulting from irreversible spin-spin interactions, is called T_2 relaxation. Because this process occurs in the transverse plane and is recorded as a complex time-domain signal, this relaxation can be modeled as a decaying sinusoidal function, and by applying a Fourier transform, this function known as free induction decay (FID) will produce an NMR spectrum in the frequency domain. The resonance frequencies of nuclei are reported as "chemical shift" values in units of parts per million (ppm), with peaks at different chemical shifts corresponding with the resonance frequency of the respective nuclei. This conversion allows for a universal method of plotting and analyzing spectra since it corrects for the fact that the resonance frequencies of nuclei scale with magnetic field strength according to the following equation:

$$Chemical\ shift\ (\delta) = \frac{(Resonance\ frequency\ of\ sample\ nucleus\ in\ Hz) - (Resonance\ frequency\ of\ standard\ in\ Hz)}{Spectrometer\ frequency\ in\ Mhz}$$

The most common reference standard used is trimethylsilane (TMS), with a chemical shift of 0 ppm. A 1D ^{1}H-NMR spectrum shows signals for each of the hydrogen atoms in a biomolecule, while a 2D NMR spectrum shows signals of hydrogen atoms that are correlated with either other hydrogen atoms or another nuclei of interest (e.g., ^{13}C, ^{15}N, etc.).

Anjum et al. (2021) shows a 1D ^{1}H-NMR spectrum of bovine Achilles tendon. Two peaks are seen in the raw 1D spectrum, with one peak centered at 0 ppm and the other peak centered at a chemical shift away from 0 ppm. Using the subband Steiglitz-McBride algorithm (SMA), these broad peaks are resolved and four peaks appear. The two peaks at 0 ppm are attributed to two pools of water present in bovine Achilles tendon, and the two peaks shifted away from the water peaks are attributed to proteoglycans and lipids. Comparing the chemical shifts obtained from the 1D spectrum to those obtained by UTE imaging of tendon (Anjum et al. 2021), the shifts are very similar. Consequently, the use of NMR spectroscopy will confirm the existence of the off-resonance components present in UTE imaging, as the UTE decay data has 16 non-linearly spaced data points that make estimates using UTE imaging less reliable than the highly sampled FID. Although the proton spectrum may provide information about the presence of the chemical shifts seen in UTE imaging, the peaks are broad due to the contribution of a variety of biomolecules that share similar chemical shifts. HR-MAS allows for a better resolved spectrum by reducing the linewidth of these broad peaks, allowing for a better assessment of the origin of off-resonance components observed in both UTE imaging data and NMR data.

d. Tendon structure and function

Tendons are an important load-bearing tissue in the musculoskeletal system, connecting muscle to bone. The composition of the tendon extracellular matrix is vital to understanding the structure and function of tendon as it comprises the vast majority of the tissue volume, and there

is a need to determine methods of monitoring changes in the extracellular matrix non-invasively in order to observe disease progression and diagnose tendinopathies. An accurate diagnosis will allow for the best clinical and therapeutic treatment of tendinopathies.

The extracellular matrix (ECM) of tendon is composed predominantly of type I collagen, which takes up the majority of dry weight in tendon (Screen et al. 2015). The collagen molecule is comprised of three polypeptide strands in a left-handed helical conformation, with a one-residue stagger between strands to form a right-handed triple helix (Shoulders and Raines, 2009). Every third residue is found to be glycine, resulting in a repeated sequence of XYGly along the length of the polypeptide chain, where X and Y can be any amino acid. The most common amino acids in the X and Y positions of the polypeptide strand are proline and hydroxyproline (Shoulders and Raines 2009). Models have been proposed since the early 1920s describing the mechanisms underlying the triple helix structure and stability. Initial models proposed the existence of direct hydrogen bonds between functional groups of amino acids comprising the collagen triple helix, while later models proposed the insertion of water bridges to stabilize the collagen triple helical structure.

These water bridges comprise the interstitial space of the collagen molecule, with the formation of these water bridges explained by electrostatics. If two oppositely charged particles exist in space, work is required to separate the particles and maintain this separation. The large separation of the hydrogen bond noted by Rich and Crick implies a higher electrostatic energy, and the Rich/Crick model of collagen structure containing a direct hydrogen bond serves as the reference point for the lowest electrostatic energy of a hydrogen bond pair. The Ramachandran model, although having a larger separation than the Rich/Crick model, proposes a water bridge that reduces the magnitude of the electrostatic energy of the hydrogen bond. When the collagen

molecule is placed in water with a dielectric coefficient of K~80, the electrostatic energy is reduced to 1/80 of the reference energy of a direct hydrogen bond. The electric dipoles of the water molecules are confined to the transverse plane of the collagen molecule, and high-resolution studies of collagen confirm that the carbonyl groups of glycine residues form single water bridges, while the carbonyl groups on proline residues in the Y position form double water bridges (Fullerton et al. 2007). These water bridges connect the main chains of collagen polypeptides and contribute to the triple helical structure of the collagen molecule.

Along with the main chain of the collagen polypeptide (i.e. amide and carbonyl groups), the side chains (i.e. R groups) of the polypeptide interact with surrounding bulk water to form a hydration layer around collagen. There is twice as much polar surface area on the side chain of the amino acids of collagen compared to the main chain, and the cooperative linking of water molecules between the main chain of amino acids in collagen and the side chain contributes to the lowest free energy state of the collagen molecule. The hydration layers formed around the collagen molecule consist of a primary hydration layer and a secondary hydration layer, with molecular weights of 0.8 grams of water/grams of dry weight (g/g) for both layers. The primary hydration layer is a result of water molecules forming hydrogen bonds with the polar regions of the collagen molecule, while the secondary hydration layer is a result of bonding to the non-polar regions of collagen. The primary hydration layer can be further divided into main chain hydration, with a weight of 0.263 g/g, and side chain hydration, with a weight of 0.54 g/g. Note that these hydration layers describe water-collagen interactions, while a lack of information exists describing the interactions and influence of other molecules on these hydration layers. These collagen molecules form fiber-like structures at different hierarchal levels; the collagen fibrils are grouped into fibers, fascicles, and finally the whole tendon. These fibrous structures

are oriented along the long axis of the tendon (the loading direction), providing tendon its significant load-bearing capabilities (Screen et al. 2015).

Interspersed between the collagen fibrils are non-collagenous matrix components, but details concerning the amount, organization, and location of these components are less well defined. Of these components, the non-collagenous proteins can be grouped into proteoglycans, glycoproteins, and glyco-conjugates (Screen et al., 2015). Proteoglycans are generally divided into two families: large aggregating proteoglycans (PGs) and small leucine-rich proteoglycans (SLRPs). SLRPs are the most abundant proteoglycan in tendon, with decorin and biglycan the two most studied class I SLRPs in tendon, followed by the class II SLRPS fibromodulin and lumican. Class I and II proteoglycans differ based on protein and genomic material, characteristic amino acid compositions, and chromosomal organization. These proteoglycans consist of glycosaminoglycan chains, specifically chondroitin sulfate and dermatan sulfate, and play a role in collagen fibril assembly, thus providing tendon its structural integrity (Screen et al. 2015). The composition and organization of all ECM components is integral to the mechanical and biological function of tendon.

The mechanical function of tendon arises from the load-bearing responsibility of tendon along the long axis. Tendons can be divided into two main types: energy storing and positional. The composition of the extracellular matrix depends on the type and function of the tendon. For positional tendons (i.e. rotator cuff tendon), decorin and biglycan between fibrils allow for fibril sliding, while energy storing tendons rely on lubrican and elastin between fascicles to enable fascicle sliding (Screen et al. 2015). Energy storing tendons stretch when experiencing a load, storing energy from the load-bearing force and returning that energy to aid in locomotion. In

addition, energy storing tendons experience strains of more than 10%, while positional tendons experience strains of around 2-3%.

The biological function of tendon stems from cell-matrix interactions within the tendon. Tendon cells govern the production and organization of the ECM, but the structure and composition of the matrix controls the cues reaching the cells. Consequently, a feedback mechanism is created to maintain tendon homeostasis and metabolic function. It is also known that the turnover rate of collagenous components in tendon is much slower than the non-collagenous components, indicating the significance of the non-collagenous components in maintaining tendon structural integrity.

e. High-Resolution Magic-Angle Spinning NMR Spectroscopy

High-resolution magic-angle spinning (HR-MAS) NMR spectroscopy proves to be an effective method for obtaining resolved spectra from samples with short relaxation times. As a result, HR-MAS is used predominantly for solids and semi-solid materials. The short relaxation times of solids and semi-solids are due in part to the limited mobility of molecules in the sample, leading to anisotropic (the property of being directionally dependent) magnetic interactions. The rapid spinning of a sample at an angle of 54.7° (the magic angle) relative to the magnetic field eliminates this chemical anisotropy according to the following equation proposed by Andrew et al. and Lowe :

$$H_D = \sum \frac{h}{8\pi^2} \gamma_i \gamma_j r_{ij}^{-3} (3 \cos^2 \theta_{ij} - 1)(I_i I_j - 3I_{iz}I_{jz})$$

In this equation, H_D is the Hamiltonian operator for dipolar coupling, I_i is the spin operator of nucleus I, and γ_I is its gyromagnetic ratio. The angle θ_{ij} is the angle between the distance vector r_{ij} between the two coupled nuclei and the magnetic field direction. For a liquid solution, the $(3 \cos^2 \theta_{ij} - 1)$ term is zero, as the molecules in a solution tumble rapidly in an isotropic

fashion, eliminating any dipolar couplings. For a solid sample, however, this term is non-zero. Spinning the sample at an angle β to the magnetic field causes the dipolar coupling to have an additional dependence of $(3cos\beta - 1)$ (Beckonert et al. 2010). Setting this term to zero, the magic angle of 54.7° is obtained, at which the dipolar couplings will be averaged to zero albeit the anisotropic nature of the sample. Other anisotropic interactions remain, including chemical shift, indirect spin-spin coupling, and magnetic susceptibility contributions. Anisotropies resulting from chemical shift and spin-spin coupling are small for ^{1}H protons, and major causes of line broadening result from magnetic susceptibility effects.

f. 2D NMR Relaxometry

NMR relaxometry differs from NMR spectroscopy in that relaxometry provides information about the bulk properties of a sample, while spectroscopy provides information about the chemical composition and structure of a sample. Although both methods can employ the same device, an NMR spectrometer, the processing of the acquired data differs between the two methods. For spectroscopy, a Fourier transform is applied to a free induction decay (FID), resulting in a spectrum in the frequency domain, while for relaxometry, an inverse Laplace transform is applied, displaying a relaxation time spectrum. Relaxometry allows one to observe the molecular dynamics of a system, as relaxation rates depend on the mobility of the microscopic environment, specifically the water environment, and the strength of the magnetic field.

A 1D NMR relaxation spectrum shows spectral peaks with axes of intensity versus relaxation time (or rate). This spectrum represents the probability distribution of finding a particular T_1, T_2, T_2* or other relaxation mechanism in the sample. Since the concentration of protons found in bulk water is the greatest pool (reservoir) of protons in biological tissue, water

peaks appear at the highest intensity in relaxation spectra. A 1D spectra is limited in that it only provides information about the relative size of each water pool present in the sample and the respective relaxation times. A 2D spectrum can be used to determine the molecular dynamics of the sample, as a 2D spectrum can be used to monitor exchange between proton species in the sample. The T_2-store-T_2 spectrum associates both time dimensions with a Carr-Purcell Meiboom-Gill (CPMG) measurement of the transverse relaxation, but allows exchange of magnetization between the proton pools by storing the magnetization in the longitudinal direction for a store time, t_2. The system of coupled differential equations governing the relaxation of magnetization of protons in the two pools is given as follows (Montelihet et al. 2006):

$$\frac{dM_a}{dt} = -k_a M_a + k_b M_b + R_a\left(M_a^{eq} - M_a\right)$$

$$\frac{dM_b}{dt} = -k_b M_b + k_a M_a + R_b\left(M_b^{eq} - M_b\right)$$

An analytical simulation of a T_2-store-T_2 spectrum of exchange between two reservoirs of protons is presented by Montelihet et al. (2006). The bottom left of this figure shows the presence of two distinct reservoirs at distinct T_2 relaxation times. The value k represents the exchange rate between the two reservoirs and t_2 represents the store period during which exchange occurs. When the store period is comparable to the exchange lifetime, cross peaks appear representing exchange between the two reservoirs in the sample (Warner 2010). This exchange can take the form of chemical exchange, in which protons are directly displaced due to the mobility of protons within a sample, or the form of magnetization exchange in which

magnetization is transferred from one reservoir to another by means of phenomena such as dipolar coupling. Looking at the graph, as the exchange lifetime changes, certain pools of protons start to disappear. At slow exchange, the proton pool with a shorter relaxation time disappears, and similarly, at fast exchange, the proton pool with a longer relaxation time disappears. By modulating the store time and observing cross peaks, the exchange lifetime of a certain sample can be determined. A model that incorporates exchange allows for a better interpretation of 1D models when exchange occurs on the time-scale of relaxation.

II.   Methods

   a. Non-MAS

      i.   Sample handling

Five fresh samples of bovine Achilles tendon were obtained from a butcher shop. Cores of the tendon were cut parallel to the collagen fibrillar structure so as to maintain the collagen fiber orientation, and placed as solid samples in 5 mm NMR tubes (Wilmad Lab, 920-2821-MW) and packed to remove any entrapped air to prevent magnetic susceptibility effects.

      ii.   Experiments

A Bruker Avance III spectrometer operating at 400 MHz was used to acquire the spectra. The spectra were recorded at a temperature of 298K and chemical shift values were recorded. The optimization and experimental protocols were conducted by an NMR core at the Department of Chemistry and Biochemistry at the Georgia Institute of Technology, without the presence of the principal investigator. A 1D ^{1}H single pulse experiment was recorded with a spectral width of 20 ppm with 64k data points; 128 scans with repetition delay of 5 s.

b. HR-MAS

i.   Sample handling

Five fresh samples of ovine Achilles tendon were obtained from a butcher shop. The

tendon was cut along the transverse axis so as to maintain the collagen fiber orientation, and a 2

mm biopsy punch (Med Vet International, BP2mm) was used to extract a sample of the tendon.

The biopsy punch was placed orthogonal to the transverse plane, and the sample was placed in a

4 mm HR-MAS insert (Bruker, B4493) for the HR-MAS experiments. One to two drops of D_2O

was added for a field lock frequency. Samples of rat rotator cuff tendon were obtained from the

subscapular region of the rat. Two samples were obtained from subscapular regions that

underwent strength testing through electric stimulation of subscapular muscle, placing cyclic

loads on the shoulder joint and rotator cuff tendon. Two control samples were obtained from the

contralateral side which did not undergo the same strength testing procedures. The rotator cuff

samples were placed in the insert by a collaborator at the Department of Biomedical Engineering

at the Georgia Institute of Technology, without the principal investigator present. One to two

drops of D_2O was added for a field lock frequency.

ii.   Experiments and Data Acquisition

For the HR-MAS experiments, a Bruker Avance III spectrometer operating at 400 MHz

with a MAS rotor frequency of 5000 Hz was used. The spectra were recorded at a temperature of

298K and chemical shift values were recorded with respect to D_2O as a reference signal at 4.7

ppm. The optimization and experimental protocols were conducted by an NMR core at the

Department of Chemistry and Biochemistry at the Georgia Institute of Technology, without the

presence of the principal investigator. 1D ^{1}H experiments were rerecorded with a spectral width

of 20 ppm, 64k data points; 128 scans with repetition delay of 5 s. 2D COSY spectral parameters

were: spectral width (f_2) = 13.0 ppm, 2048 complex points; spectral width (f_1) = 13.0 ppm, 128 t_1

increments with 64 scans per t_1 value; repetition delay = 2.0 s. 2D HSQC parameters were:

spectral width (f_2) = 13.0 ppm, 2048 complex points; spectral width (f_1) = 220 ppm, 256 t_1

increments with 64 scans per t_1 value; repetition and evolution delay = 1.5 s and 0.2 ms,
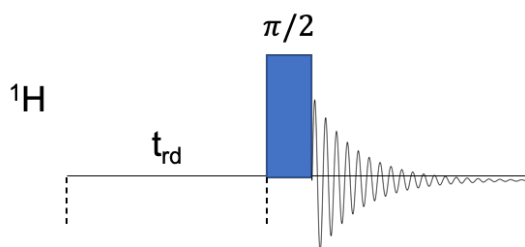
respectively.

Figure 1. 1H pulse acquire. This pulse sequence consists of a recycling delay t_{rd} followed by a 90 pulse and the acquisition time. During the recycling delay, a water suppression sequence is used to eliminate water proton signals in the sample. The spectrum generated from this sequence provides chemical shift information about protons (^{1}H) in the sample.
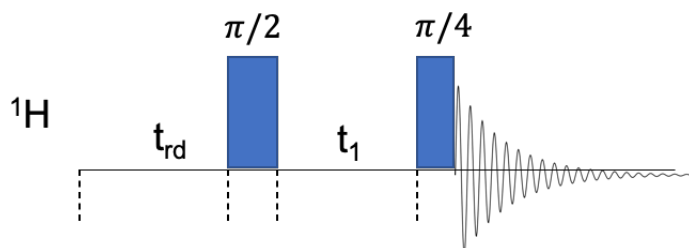

Figure 2. COSY. This sequence involves a recycling delay time t_{rd}, followed by a 90° pulse, a delay time t_1, a 45° pulse, and acquisition time. The angle of the second pulse can be adjusted to obtain the best signal to noise ratio, with an angle of 45° being the optimal angle. The spectrum generated by this sequence shows homonuclear (^{1}H-^{1}H) couplings.
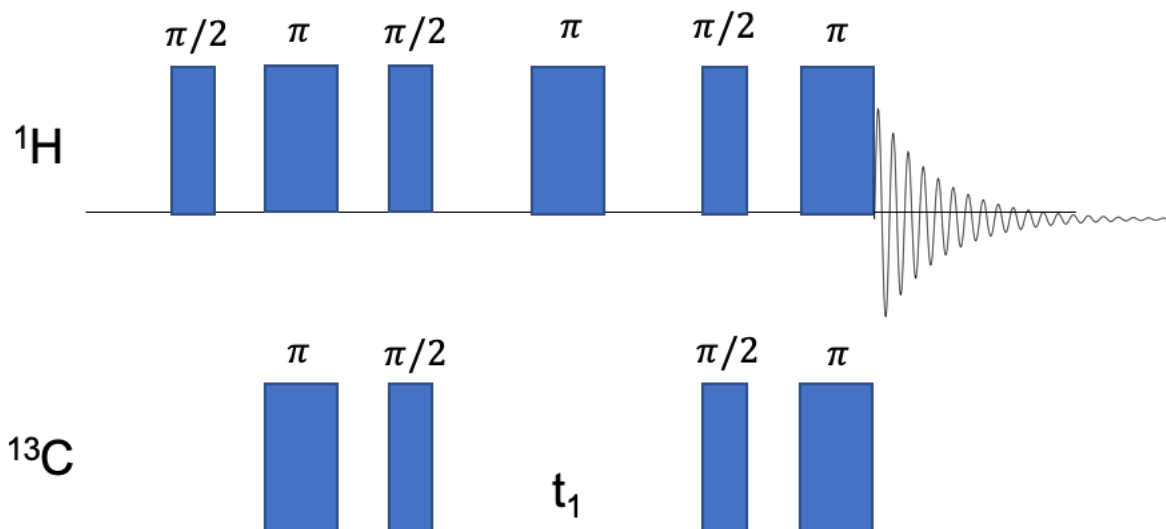
Figure 3. HSQC. This sequence transfers proton magnetization to ^{13}C, records ^{13}C chemical shift information, and transfers magnetization back to protons and records proton chemical shift information. With this sequence, coupling between protons and carbons to which they are attached can be determined.

    iii.   Processing and peak assignments

The spectra were processed using MestreNova Version 14.2.0 (Mestrelab, Spain) and optimized with a full auto Bernstein Polynomial baseline correction, an exponential apodization of frequency 0.3 Hz and line width 0.932 Hz, and auto first-order phase correction. An auto multiplet analysis and auto peak integration was used, and peak assignments were made based on existing literature on cartilage, as cartilage has a composition and relaxation properties similar to that of tendon, and the Human Metabolome Database (HMDB).

c. NMR relaxometry

    i.   Sample handling

Fresh samples of ovine Achilles tendon and bovine Achilles tendon were obtained from a butcher shop. Cores of the tendon were cut parallel to the collagen fibrillar structure so as to maintain the collagen fiber orientation, and the samples were placed in 5 mm high resolution

NMR tubes (Wilmad-Lab, 920-28126-MW). The samples were placed in the tubes without homogenization and without the addition of solvent, with care taken to prevent the entrapment of air so as to reduce any magnetic susceptibility artifacts. Samples were sealed in the NMR tubes to avoid loss of fluid to the air.

ii.   Experiment

The experiment conducted was a T_2-store-T_2 experiment defined by the pulse sequence below, with a store period of t_m:
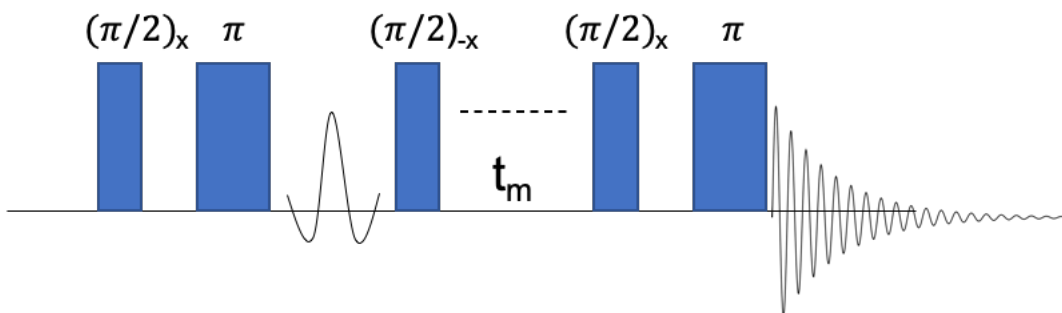

Figure 4. Pulse sequence for T_2-store-T_2 relaxometry.

iii.   Data acquisition

The data was acquired on a Bruker NMR spectrometer operating at 400 MHz, and the optimization and experimental protocols were conducted by an NMR core at the Department of Chemistry and Biochemistry at the Georgia Institute of Technology, without the presence of the principal investigator. The data was acquired at 298K with a spectral width of $f_2 = 250$ ppm and $f_1 = 10$ ppm, with 1024 linearly spaced (TE = 25 µs) and 32 non-linearly spaced real points in the direct and indirect dimensions, respectively. The repetition time was 4 s, with mixing times (i.e. store periods) of 1, 10, and 100 ms, and the number of sample acquisitions was 4.

The data was processed using MATLAB (Mathworks, U.S.A.) with a 2D ILT program (Callaghan et al. 2003) and a 2D subband SMA program (Anjum et al. 2021, ISMRM abstract).

III.   Results

a.   Non-MAS spectroscopy

Figure 5 shows a ^{1}H spectrum of bovine Achilles tendon, acquired using the pulse sequence and spectral parameters described in Figure 1. The top of the figure shows the raw spectrum of bovine Achilles tendon, while the bottom of the figure shows a deconvolved spectrum using SMA. The deconvolved spectrum shows the presence of two peaks centered at 0 ppm, and two off-resonance peaks with chemical shifts of -2.7 and -3.4 ppm. These peaks are similar to the chemical shifts of the off-resonance components obtained from UTE imaging of -2.9 and -3.9 ppm (Anjum et al. 2021). Adjusting the chemical shift of water to 4.7 ppm, the off-resonance peaks in the ^{1}H NMR spectrum have chemical shifts of 2.0 and 1.3 ppm.
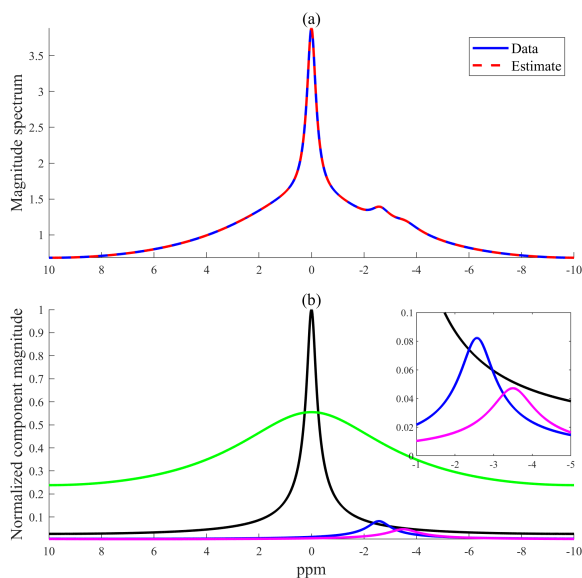

Figure 5. (a) Proton NMR spectrum of bovine Achilles tendon (blue trace) with fit result using SMA (red trace). (b) Individual spectral components obtained using SMA, showing a prominent

water peak at 0ppm and two off-resonance peaks at -2.7 ppm and -3.4 ppm. (SMA = sub-band Steiglitz-McBride algorithm)

b. HR-MAS spectroscopy

i.   Ovine Achilles tendon

Figure 6 shows a 1D HR-MAS ^{1}H spectrum of ovine Achilles tendon. Compared to the

non-MAS ^{1}H spectrum of bovine Achilles tendon (Figure 5), the spectrum acquired using HR-

MAS shows the existence of more distinct peaks in the region of 0 to 3 ppm. Additional peaks as

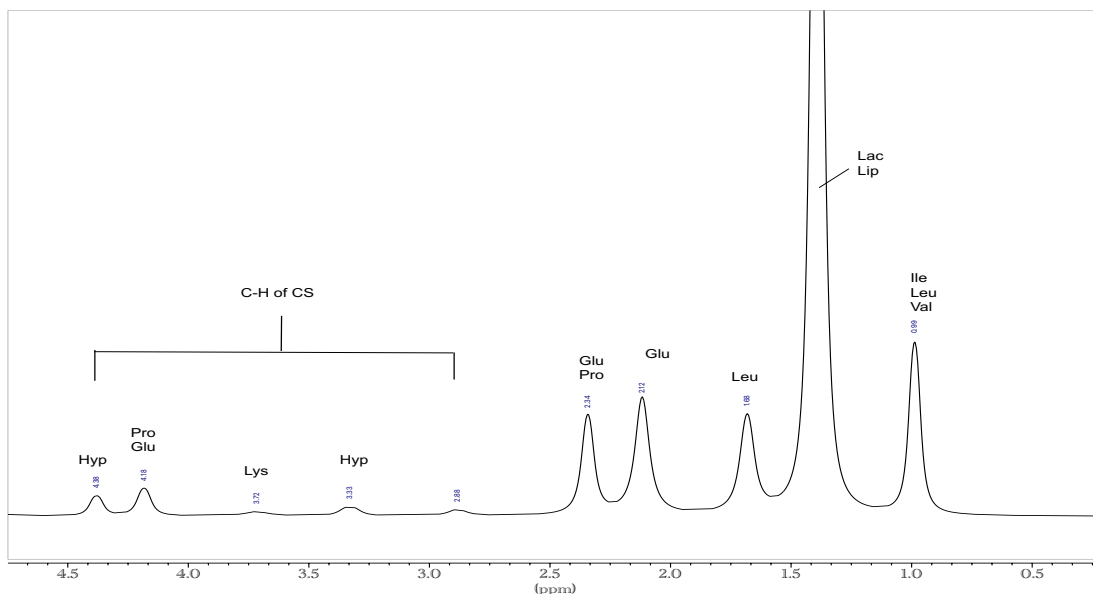compared to the non-MAS spectrum can be seen in the region of 3 to 5 ppm.

Figure 6. HR-MAS proton spectrum of ovine Achilles tendon with preliminary peak assignments. Abbreviations correspond to the three letter code for amino acids. (Lac = lactate, lip = lipid).

Tables 1 and 2 provide the chemical shift of protons (^{1}H) and carbon (^{13}C) observed in

both ovine Achilles tendon and rat rotator cuff tendon. Looking at the chemical shifts seen in

ovine Achilles tendon, the broad peak observed at 0.96-0.99 ppm is attributed to leucine,

isoleucine, valine, and lipids. Preliminary assignments are made by looking only at the 1D

spectra, but the presence of different biomolecules sharing similar chemical shifts in this peak

region necessitates the use of 2D experiments to distinguish between the shared resonances of these biomolecules. Looking at the 2D HSQC spectrum (Figure 7), the shifts observed at 0.96-0.99 ppm are attributed primarily to isoleucine and lipids based on the detection of cross peaks correlating the proton chemical shifts with their respective carbon chemical shifts (Tables 1 and 2).

Table 1. ^{1}H Chemical Shifts of ovine Achilles tendon and rat rotator cuff tendon

Ovine Achilles tendon		Rat rotator cuff tendon	
Chemical shift (ppm)	Preliminary assignment	Chemical shift (ppm)	Preliminary assignment
0.96-0.99	Ile, Leu, Val, Lip	0.91, 0.98	Ile, Leu, Val
1.38	Lip	1.19	Ile
1.68	Leu	1.34	Lac
2.12	Glu	2.06	Pro, Hyp
2.34	Pro, Glu	3.05	Lys
3.33	Hyp	3.29	His
3.72	Lys	3.95	Gly
4.18	Pro, Glu	3.0 – 5.0	C-H of CS
4.37	Hyp	4.13	CH$_2$ in glycerol backbone
3.0-5.0	C-H of CS	-	-
5.41	O-H of CS	-	-

Table 2. ^{13}C chemical shifts of ovine Achilles tendon and rat rotator cuff tendon

Ovine Achilles tendon		Rat rotator cuff tendon	
Chemical shift (ppm)	Preliminary assignment	Chemical shift (ppm)	Preliminary assignment
13.43	Ile, Lip	13.65	Fatty acid/acyl terminal -CH3
24.37	Leu	21.80	Lac
26.73	Glu	23.62	Ile

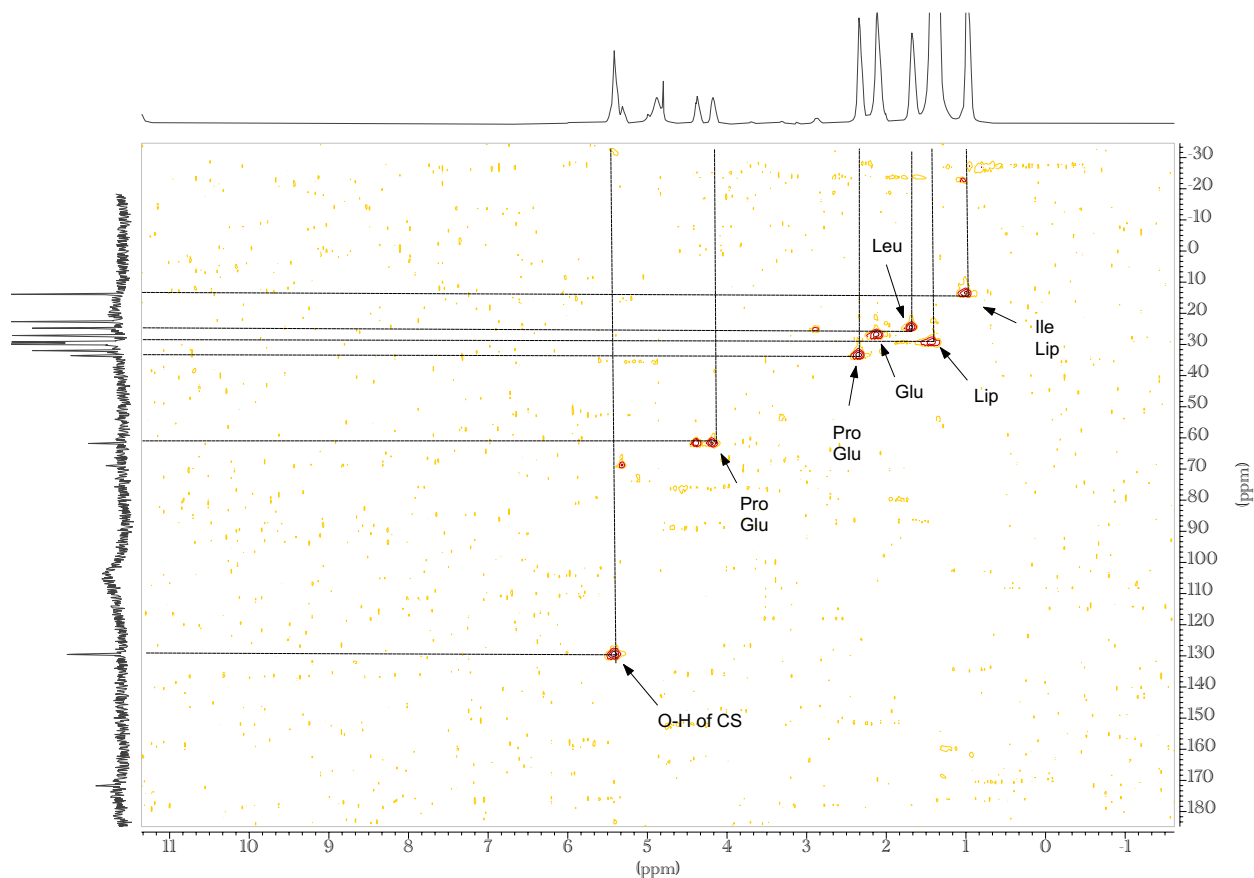|			
29.09	-CH2-, fatty acid/acyl	27.38	Pro
33.17	Pro, Glu	39.18	Lys
61.49	Pro, Glu	68.35	C-2, glyceryl residues
129.27	O-H of CS		

Figure 7. 2D HSQC spectrum of ovine Achilles tendon. Peaks represent protons coupled to their respective attached carbons.

The proton chemical shifts observed at 2.12 and 2.34 ppm are attributed to glutamate, the shifts at 2.34 ppm and 4.18 ppm are attributed to proline, and those at 3.33 and 4.37 ppm are attributed to hydroxyproline. The shifts ranging from 3.0 – 5.0 ppm, assigned to the aforementioned amino acids, share overlapping peaks with resonances from the C-H protons of

chondroitin sulfate. Chondroitin sulfate comprises the GAG chains of decorin and biglycan, members of the SLRP family of proteoglycans found in tendon.

        ii.   Rat rotator cuff tendon

Figure 8, along with tables 1 and 2, show chemical shifts at 0.91 and 0.98 ppm attributed to isoleucine, leucine, and valine. In addition, the peak at 1.19 ppm is also attributed to isoleucine. The substantial peak at 1.34 ppm is attributed to overlapping peaks of lactate and lipid.
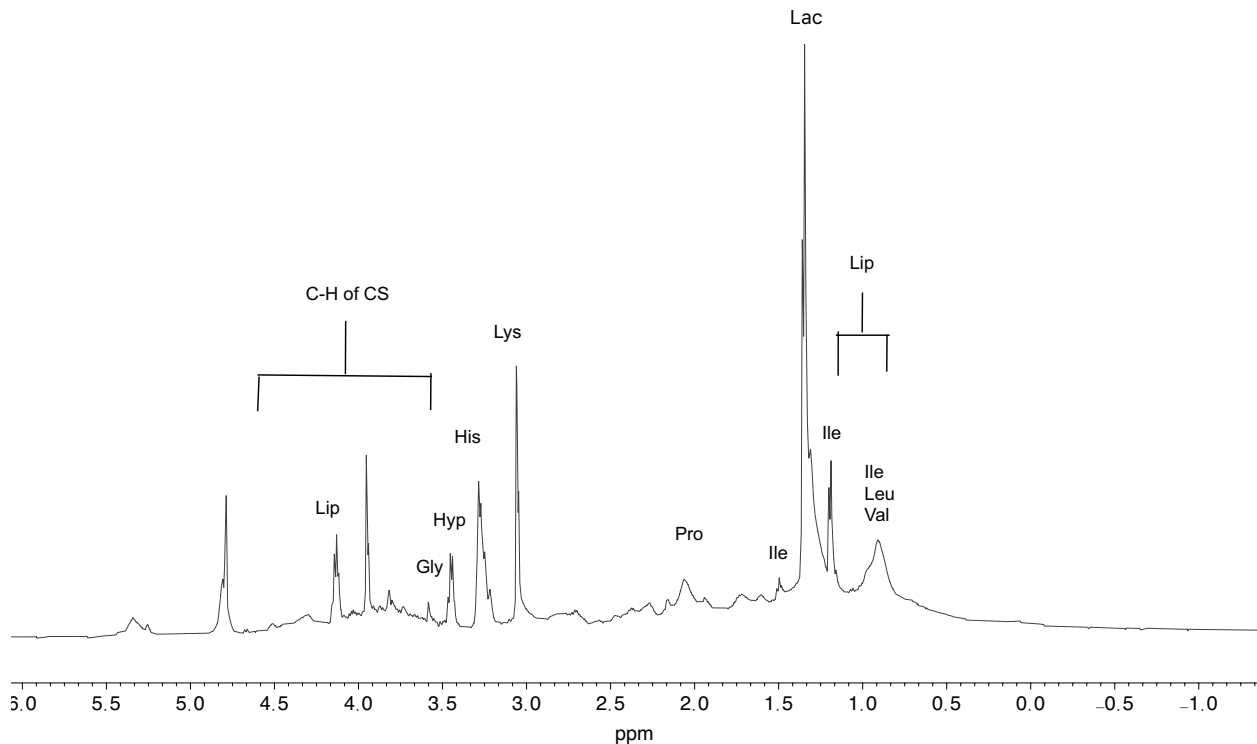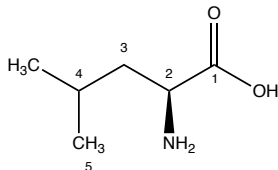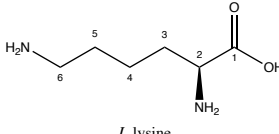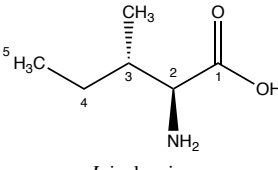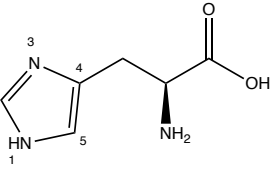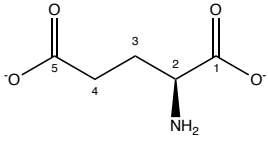

Figure 8. HR-MAS proton spectrum of rat rotator cuff tendon with preliminary peak assignments. Abbreviations correspond to the three letter code for amino acids. (Lac = lactate, lip = lipid, CS = chondroitin sulfate)

The peak at 2.06 ppm is attributed to proline and hydroxyproline, the two most common acids comprising the collagen triple helix. The peak at 3.05 ppm is lysine, which is an amino acid
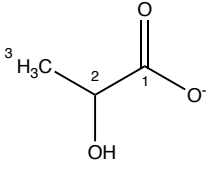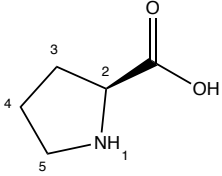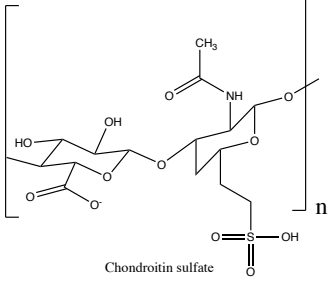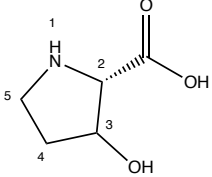
integral to collagen synthesis. The peak at 3.29 ppm is attributed to histidine, an amino acid found in collagen that participates in cross-linking with lysine and hydroxylysine to maintain the structural integrity of the collagen triple helix (Yamauchi et al. 1987). The peak at 3.57 ppm is attributed to glycine, which is the most abundant amino acid found in the collagen peptide chain. The protons to which these peaks are assigned to for each compound are given in Table 3 for both tendons.

Table 3. Chemical Structures and ^{1}H Chemical Shifts of Biomolecules Detected in Nuclear Magnetic Resonance (NMR) Spectrum of Bovine Achilles and Rat Rotator Cuff Tendon

Structure	Shifts	Structure	Shifts
L-leucine	(2) = 3.75 (3) = 1.71 (4) = 1.71 (5) = 0.95 (6) = 0.94	L-lysine	(1) = 3.74 (2) 1.89 (3) = 1.44 (4) = 1.70 (5) = 3.01
L-isoleucine	(2) = 3.67 (3) = 1.97 (4) = 1.46/1.25 (5) = 0.92 (6) = 1.00	L-histidine	(2) = 3.16 (5) = 3.23 (6) = 3.98 (7) = 7.09
L-glutamate	(2) = 3.77 (3) = 2.06 (4) = 2.34	Lactate	(2) 4.12 (3) = 1.32

L-proline	(2) = 4.13 (3) = 2.35/2.08 (4) = 2.01 (5) = 3.43/3.34	Chondroitin sulfate	3.0 – 5.0
Hydroxyproline	(2) = 4.35 (3) = 2.43/2.17 (4) = 3.50 (5) = 3.37	-	-

The peak at 4.13 ppm is attributed to the CH_2 protons of the backbone of glycerol. The peaks ranging from 3.0 – 5.0 ppm are attributed to the C-H protons of chondroitin sulfate, similar to the peaks observed in ovine Achilles tendon.

c. NMR relaxometry

The 2D relaxometry spectra of rat rotator cuff, ovine Achilles, and bovine Achilles tendon show two pools of protons with distinct relaxation times (Figures 9-11). At a short mixing time of 1 ms, two distinct pools of water with different relaxation times can be observed along the diagonal for all tendons. At a mixing time of 10 ms, cross peaks start to appear off the diagonal that correspond to exchange between the two distinct pools of water. At 100 ms, the peak with the greater relaxation time starts to disappear, and cross peaks remain. This exchange rate can be determined by quantifying the amplitude buildup of the cross peaks with mixing times and fitting the data to the ILT model. As the exchange rate approaches the mixing time, the intensities of the cross peaks reach a maximum. However, non-parametric methods like the ILT,

while providing qualitative information on inter-compartmental exchange, are not always optimal for quantifying exchange rates and thus a parametric method can provide more reliable estimates. As a result, a parametric method of determining the exchange is used. Figure 12 shows the spectra obtained from the 2D subband Steiglitz-McBride algorithm, in which exchange and relaxation rates can be quantified (Anjum et al. 2021; Woessner et al. 1996). Using this algorithm, for bovine Achilles tendon, the exchange rate is determined to be 0.2532 ms^{-1}; for the ovine Achilles tendon, the exchange rate is determined to be 0.3602 ms^{-1}; and for the rat rotator cuff tendon, the exchange rate is determined to be 0.1584 ms^{-1}. The respective relaxation rates of both water pools in each tendon is similar in both the 2D ILT and 2D SMA analysis. The ILT analysis is presented in a log scale, whereas the SMA analysis is presented in a linear scale, so a comparison of both methods requires the conversion of the log scale in ILT to a linear scale. The relaxation rate (i.e., 1/relaxation time) of the long component in bovine Achilles, ovine Achilles, and rat rotator cuff tendon are 0.84, 0.31, and 1.49 ms^{-1}. The relaxation rate of the short component in bovine Achilles, ovine Achilles, and rat rotator cuff tendon are 0.06, 0.09, and 0.03 ms^{-1}. The variance of each estimate is low, showing the robustness of the SMA analysis.
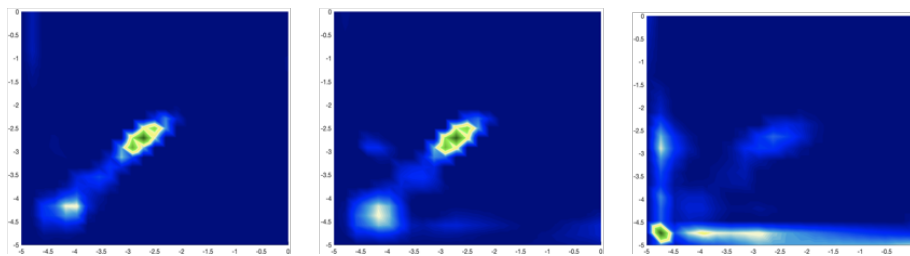

Figure 9. 2D ILT spectra of rat rotator cuff tendon. Peaks on the diagonal correspond to distinct pools of water in tendon with different relaxation rates. Cross peaks represent exchange between the water pools. The mixing times as displayed from left to right are: t_m = 1, 10, and 100 ms.
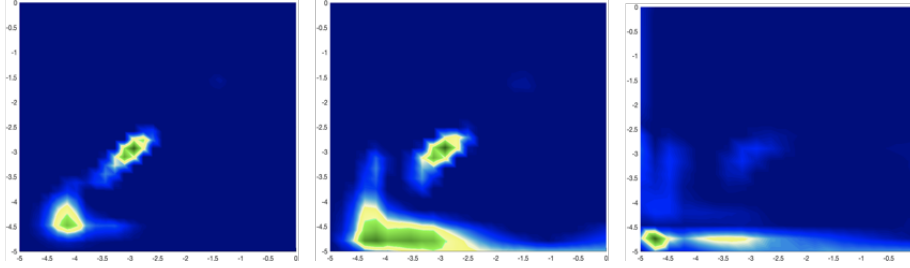
Figure 10. 2D ILT spectra of ovine Achilles tendon. Peaks on the diagonal correspond to distinct pools of water in tendon with different relaxation rates. Cross peaks represent exchange between the water pools. The mixing times as displayed from left to right are: t_m = 1, 10, and 100 ms.

Figure 11. 2D ILT spectra of bovine Achilles tendon. Peaks on the diagonal correspond to distinct pools of water in tendon with different relaxation rates. Cross peaks represent exchange between the water pools. The mixing times as displayed from left to right are: t_m = 10 and 100 ms.

Figure 12. 2D SMA spectra of bovine Achilles, ovine Achilles, and rat rotator cuff tendon. Peak Peaks on the diagonal correspond to distinct pools of water in tendon with different relaxation rates. Cross peaks represent exchange between the water pools. The mixing times as displayed from left to right are: t_m = 1, 10 and 100 ms.

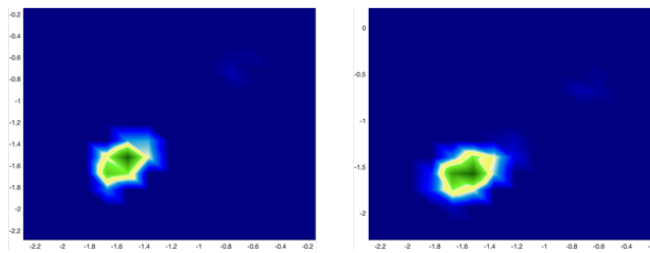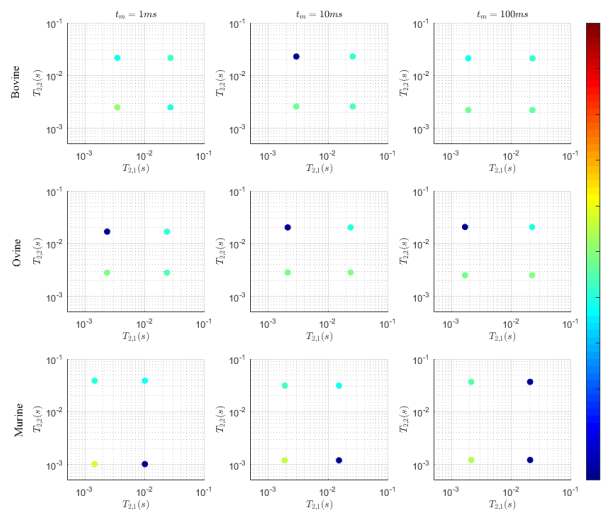Table 4. Exchange-rate estimates of T2-T2 NMR relaxometry data and apparent and inherent bi-component estimates of proton NMR data of bovine (Achilles), ovine (Achilles), and murine (rotator cuff) tendon.

Group	Method	Specimen	1	2	3	MEAN	STD
MURINE	FID	M_b	0.3107	0.2504	0.3563	0.3058	0.0531
		M_a	0.6524	0.7214	0.6171	0.6636	0.0530
		$R_{2,b}$ (ms^{-1})	0.0385	0.027	0.0186	0.0280	0.0099
		$R_{2,a}$ (ms^{-1})	1.4199	1.6501	1.3952	1.4884	0.1406
	T2-T2	λ_{eff} (ms^{-1})	0.1793	0.1171	0.1788	0.1584	0.0358
OVINE	FID	M_b	0.1809	0.3537	0.2203	0.2516	0.0906
		M_a	0.7938	0.6258	0.7724	0.7307	0.0914
		$R_{2,b}$ (ms^{-1})	0.1088	0.0882	0.0685	0.0885	0.0202
		$R_{2,a}$ (ms^{-1})	0.3334	0.3827	0.2003	0.3055	0.0944
	T2-T2	λ_{eff} (ms^{-1})	0.3944	0.3422	0.3440	0.3602	0.0296
BOVINE	FID	M_b	0.4163	0.1300	0.1015	0.2159	0.1741
		M_a	0.5283	0.8262	0.8235	0.7260	0.1712
		$R_{2,b}$ (ms^{-1})	0.0861	0.0539	0.0492	0.0631	0.0201
		$R_{2,a}$ (ms^{-1})	0.8695	0.9183	0.7202	0.8360	0.1032
	T2-T2	λ_{eff} (ms^{-1})	0.2771	0.2475	0.2351	0.2532	0.0216

IV.   Discussion

Prior peak assignments have been made in related connective tissues like cartilage using HR-MAS (Ling et al. 2007; Schiller et al. 2001; Borel et al. 2008; HMDB). Although cartilage and tendon have different functional properties, they are comprised of similar matrix constituents and cellularity. Both cartilage and tendon are composed of collagen fibrils, with cartilage having primarily type II collagen as opposed to the abundance of type I collagen in tendon. Collagen I and II differ in their hierarchal organization, with type I collagen having a more defined hierarchy and conferring greater rigidity and tensile strength. However, the amino acid composition of the triple helices comprising both tendon are similar, and so the existence of peaks in tendon that corroborate with peaks attributed to collagen observed in cartilage provides a guide to characterizing the tendon matrix composition. The proteoglycans present in both tissues also share similarities, with both tissues containing chains of chondroitin sulfate. Peak assignments are also made based on prior literature on chondroitin sulfate and lipids, specifically cholesterol esters and triglycerides (Li et al. 2017; Mucci, Schenetti, and Volpi 2000; HMDB). Using this prior literature in combination with knowledge of tendon matrix composition based on biochemical and histological studies, peak assignments were made to the chemical shifts observed in ovine Achilles and rat rotator cuff tendon.

a.   Ovine Achilles tendon

The isoleucine and leucine are derived from the small leucine-rich proteoglycans (i.e. decorin and biglycan) present in tendon. Decorin and biglycan play an integral role in the maintenance and integrity of the tendon extracellular matrix, allowing for fibril sliding and contributing to the tensile strength of tendon. The lipids may be derived from circulating low-density lipoproteins (LDLs), which carry triacylglycerides (TAGs) and cholesterol esters and

deposit them in non-liver tissues. The presence of lipids in tendon has been observed in both human and animal models, in which subjects that were exposed to a high cholesterol diet developed tendinopathies. Excessive dietary lipids may cause an increase in weight, placing greater stress on tendon leading to tendinopathies, or result in dyslipidemia. Dyslipidemia occurs when oxidized LDLs alter the gene expression of tenocytes, resulting in reduced collagen I expression and increased metalloprotease expression (Scott et al. 2014). Matrix metalloproteinases (MMPs) are enzymes produced by tenocytes that break down tendon extracellular matrix components, and an overexpression of these proteins causes abnormal tendon degradation leading to tendon weakness and subsequent tendinopathy (Buono et al. 2013).

The existence of glutamate within tendon is associated with tendinopathic features, as there exists a non-neuronal glutamate system in tendons with observed tendinopathy. *In vitro* studies of tendon cells cultured with high concentrations of glutamate have shown increased cell death and decreased cell viability, and exposure to glutamate decreases the RNA level of scleraxis, a transcription factor vital to the production and maintenance of tenocytes. In addition, increased loading of tendon, which is often a factor for the development of tendinopathy, has been shown to increase the levels of glutamate production within tendon (Spang et al. 2017). Although glutamate is detected, the intensity of the peak is small and thus may not signify tendon injury, since the ovine Achilles tendon represents a healthy model of tendon. Hydroxyproline and proline are important amino acids comprising the collagen triple helical structure, as the ring structure of both amino acids imposes a motional constraint that causes kinks contributing to the wound helical structure.

b. Rat rotator cuff tendon

The presence of lactate has been observed in injured tendons. Lactate, a product of anaerobic glycolysis, has been shown to stimulate collagen production in tenocytes following tendon injury (Hunt et al. 1978). Tendon injury leads to a hypoxic ECM environment, thus stimulating anaerobic glycolysis in tenocytes. In addition, studies by Comstock and Udenfriend (1970) show that lactate stimulates the enzyme proline hydroxylase, which is responsible for collagen synthesis and repair. Lactate concentrations have also been shown to remain elevated as the tissue returns to a normal, oxygenated state due to the conversion of TCA intermediates into lactate. Consequently, the presence of lactate may indicate prior tendon injury and subsequent repair.

During the formation of the collagen triple helix, lysine is hydroxylated allowing for cross-linking and subsequent glycosylation by galactose and glucose. The cross-linking maintains the helical structural integrity, and glycosylation allows for cell-collagen interactions and the development of collagen signaling pathways, maintaining the biological function of the tendon ECM (Yamauchi and Sricholpech 2012).

Chemical shifts attributed to glycerol are observed in rat rotator cuff tendon. Glycerol is the primary constituent of TAGs, in which three fatty acyl chains are attached to a glycerol backbone. TAGs are transported by LDLs and are found in tendons with observed tendinopathy.

c. Comparison of ovine Achilles tendon to rat rotator cuff tendon

Comparing the chemical shifts and spectra of ovine Achilles tendon and rat rotator cuff tendon, the composition of both tendons share many similarities. Both tendons have peaks attributed to amino acids comprising collagen molecules, as well as peaks attributed to amino acids comprising lipids and proteoglycans present in the interfibrillar matrix between the

collagen fibrils. Despite these similarities, there exist differences between the spectra of both tendons arising from a number of factors, listed from most likely to least likely:

(1) **Functionality of tendons.** The ovine Achilles tendon is an energy-storing tendon, undergoing large amounts of stress and force, while the rat rotator cuff tendon is a positional tendon and therefore experiences significantly less stress than energy-storing tendons.

(2) **Treatment of tendons prior to sample handling**. Since the ovine Achilles tendon was obtained from a butcher shop, it can be assumed that the sheep was raised on a farm prior to slaughter, subjected to farm practices. The rat rotator cuff tendon was obtained from rats that were raised in a lab. These rats were subjected to surgical treatments inducing subscapular injuries, followed by extensive muscle-tendon force testing to evaluate muscle strength changes with an injury model of rat. The muscle activation was performed using electrical stimulation.

(3) **Resolution of spectra.** The resolution of the rat rotator cuff tendon is much better than the resolution of the ovine Achilles tendon, as is observed by the narrower line widths, revealing more structural information about the tendon. Prior literature has shown that cartilage digestion leads to richer, more resolved spectra (Schiller et al. 2001). Comparing the treatment of tendons prior to sample handling, the rat rotator cuff tendon was derived from a rat tendon injury model subjected to significant force testing before excision. This force testing, along with tendon injury, may have resulted in collagen and ECM degradation, providing a richer spectrum for the rat compared to the ovine, in which the animal only underwent farm practices and was expected to have a healthy, uninjured tendon. In addition, since the Achilles tendon is

an energy-storing tendon, the amount of force required for tendon degradation is significantly higher than the force required for the degradation of the rotator cuff tendon. Thus, broader lines observed in the ovine AT are expected in comparison with the rat tendon.

(4) **Confounding factors during sample handling.** When excising the rat tendon, there may have been muscle excised along with the tendon due to the proximity and large size of muscle in comparison to rat tendon. Consequently, peaks attributed to biomolecules found within tendon could potentially arise from metabolites and biomolecules present within muscle tissue.

d. NMR relaxometry

Looking at the data, the exchange rate for bovine and ovine Achilles tendon is similar, while the rat rotator cuff tendon is lower. This may be attributed to the functional role of the tendons, as the Achilles tendon is load-bearing while the rotator cuff tendon is positional, or differences in a healthy versus injury model of tendon.

Comparing the spectra generated using a 2D inverse Laplace transform (ILT) compared to the spectra generated using 2D SMA, the relaxation rates determined by both methods are fairly similar. For direct comparison, the ILT analysis which presents the data in a log scale must be converted to a linear scale by raising 10 to each value on the ILT axis (i.e., -2 corresponds to 10^{-2}). The primary difference between the two processing methods is that the ILT is a non-parametric transform domain method, whereas the SMA is a parametric transform domain method. The ILT shows shorter relaxation rates compared to the SMA, but the SMA provides a more robust and reliable method for quantification of exchange and relaxation rates. The table of relaxation values from SMA are the inherent relaxation values of the water pools in tendon,

whereas ILT provides the apparent relaxation values of the water pools in tendon. Consequently, the values determined by ILT provide an underestimate of the true relaxation and exchange rates of tendon.

V.   Conclusion

UTE imaging has been used to image samples with very short relaxation times. For biological tissue, this consists of cartilage, tendon, and bone amongst others. UTE imaging was used in this study to examine human Achilles tendon, with a multi-component model fitted to the decay data. From this model, two distinct relaxation times were observed, attributed to water within the tendon, along with two off-resonance components attributed to lipids and proteoglycans. The presence of these off-resonance components was also observed in a 1D deconvolved proton spectrum of bovine Achilles tendon, necessitating further studies to determine the origin of these off-resonance peaks. The use of HR-MAS NMR spectroscopy allowed for the characterization of NMR signals present in tendon, while NMR relaxometry allowed for a clearer interpretation of relaxation times associated with the two observed pools in tendon, which were determined to be in exchange.

Using HR-MAS NMR spectroscopy, preliminary assignments were made to peaks observed in the spectrum. Peaks of interest included those attributed to the amino acids that comprise the SLRP family of proteoglycans in tendon, along with amino acids that comprise the structure of the collagen fibrils. Such amino acids include leucine and isoleucine, proline and hydroxyproline, lysine, and histidine. These amino acids are assumed to exist in a bound form in tendon, with the visibility of these NMR signals arising from the mobility of proteoglycans in the ECM and the mobility of certain amino acids (e.g. proline, lysine, etc.) comprising the collagen fibrils. Other peaks of interest included those attributed to lipids, specifically those of protons on

the alkyl/acyl chains of fatty acids. These peaks were assigned based on 2D spectra, as the one dimensional spectra had lipid peaks that overlapped with chemical shift values of collagen and proteoglycans. Peaks ranging from 3.0 – 5.0 ppm were attributed to protons of chondroitin sulfate, but were of lower intensity and were not well defined. Further investigations involving the digestion of tendon may provide better resolved and more intense peaks in this range, allowing for better characterization of the proteoglycans (i.e. GAG chains) present in the tendon ECM. A major peak of interest was lactate, since the role of lactate and its quantification in tendon is not well studied. However, the presence of lactate may be due to confounding factors including unwanted muscle tissue in the sample and force testing prior to sample handling and data collection.

Using NMR relaxometry, the relaxation times and exchange rate of proton pools in tendon was determined. Two models were used to generate T_2-store-T_2 relaxometry spectra of tendon: 2D inverse Laplace transform and 2D subband Stieglitz-McBride algorithm. The 2D inverse Laplace transform showed the presence of two water proton pools with distinct relaxation times, and the presence of exchange was observed as the mixing time increased. These water proton pools were attributed to the fast relaxation of interstitial water between collagen fibrils, and the slow relaxation of bulk water comprising the hydration layer around tendon and water in the interfascicular matrix. 2D ILT provided a qualitative assessment of relaxation times and exchange rates observed in tendon, but wasn't optimal in quantifying exchange rates due to a non-parametric method of fitting. 2D SMA, a parametric method, allowed for a quantitative determination of exchange rates and relaxation times, and when compared to relaxation times determined from 2D ILT, it was found that relaxation times using ILT were underestimates of the true relaxation times observed in tendon.

Results from HR-MAS spectroscopy and NMR relaxometry help to better understand the models used to interpret data from UTE imaging of tendon. The multi-component model fitted to UTE decay data from tendon detected the presence of two off-resonance components to water and were attributed to lipids and proteoglycans. The preliminary peak assignments made to spectra acquired from HR-MAS NMR detected resonances attributed to proteoglycans and lipids at chemical shifts equivalent to those observed in the UTE decay data. This shows the ability of using a multi-component model in UTE imaging of tendon to assess tendon structural integrity and potential tendinopathy. In other words, changes in the amplitudes of these off-resonance components may be used to develop diagnostic biomarkers for tendinopathy.

The use of NMR relaxometry also helps to better understand the relaxation rates determined by bi-component and multi-component fitting of UTE decay data. Exchange between two pools of water protons can be grouped as follows: fast exchange, when the exchange rate is greater than the average of the relaxation rates of the two pools; slow exchange, when the exchange rate is lower than the average of the relaxation rates of the two pools; and intermediate exchange, when the exchange rate is similar to the average of the relaxation rates of the two pools. If the pools of water protons are in slow exchange, a bi-exponential model may provide a robust method of determining distinct relaxation times of the two proton pools in tendon. If the proton pools are in fast exchange, a mono-exponential model may provide the most robust method of determining a single relaxation time that is attributed to the average of the relaxation times of the two pools of protons. Using NMR relaxometry, it is determined that the two pools in tendon are in intermediate exchange. Prior studies have used the short T_2* (fast relaxing) component to interpret changes in water content and collagen fiber orientation in Achilles tendinopathy (Woessner et al. 1996) through a bi-exponential fit. However, in the presence of

exchange, this short component is underestimated using the bi-exponential model, with the longer (slower relaxing) component and other parameters describing both water pools as overestimated. Consequently, a bi-exponential model may fail to correctly estimate the true relaxation times observed in tendon, and care must be taken in interpreting the relaxation times determined by a bi-exponential model used to analyze UTE decay data from tendon. The multi-component model, with the detection of off-resonance components, provides a more robust method of determining relaxation times of the two water pools. However, similar to the bi-exponential model, the multi-component model suffers from identifying the true relaxation times of water pools in tendon. Therefore caution must be taken when using the relaxation times of water pools in tendon to assess tendon structural integrity, and evaluation of the amplitudes of off-resonance components may provide a more accurate assessment of tendon structural integrity and tendinopathy.

Further investigations will include acquiring spectra of the muscle tissue surrounding the rat rotator cuff tendon and comparing it to rat rotator cuff spectra analyzed in this study to determine the presence of overlapping peaks and potential errors in peak assignments. Investigations will also include acquiring spectra of rat tendon from other regions of the rat (e.g., rat tail tendon) and spectra from tendon that has not undergone strenuous force testing. Currently, an IRB protocol has been submitted to obtain human surgical waste from upper extremity surgeries to examine the composition of human rotator cuff tendon and muscle tissue. Finally, mass spectrometry experiments will be conducted to validate the presence of certain proteoglycans and lipids assigned to peaks in NMR spectra of tendon. The tendon will need to be digested with chaotropic or detergent based agents and analyzed using LC/MS.

Overall, this study was able to identify NMR signals attributed to tendon ECM components and observe the presence of exchange between the two pools of water found in tendon. The results of this study will provide a better interpretation of models used to examine tendon and develop potential quantitative biomarkers of tendon structural integrity, especially in tendons with observed tendinopathies. These biomarkers may aid in better clinical and therapeutic strategies to treat tendon pathologies.

VI.   References

Andrew, E., Bradbury, A., and Eades, R. Removal of Dipolar Broadening of Nuclear Magnetic Resonance Spectra of Solids by Specimen Rotation. *Nature* 183**:** 1802–1803. https://doi.org/10.1038/1831802a0.

Anjum, Muhammad A.R., Felix M. Gonzalez, Anshuman Swain, Johannes Leisen, Zahra Hosseini, Adam Singer, Monica Umpierrez, and David A. Reiter. 2021. "Multi-Component T2∗ Relaxation Modelling in Human Achilles Tendon: Quantifying Chemical Shift Information in Ultra-Short Echo Time Imaging." *Magnetic Resonance in Medicine*, no. December 2020: 415–28. https://doi.org/10.1002/mrm.28686.

Beckonert, Olaf, Muireann Coen, Hector C. Keun, Yulan Wang, Timothy M.D. Ebbels, Elaine Holmes, John C. Lindon, and Jeremy K. Nicholson. 2010. "High-Resolution Magic-Angle-Spinning NMR Spectroscopy for Metabolic Profiling of Intact Tissues." *Nature Protocols* 5 (6): 1019–32. https://doi.org/10.1038/nprot.2010.45.

Bi, Yuying, Prabir Patra, and Miad Faezipour. 2014. "Structure of Collagen-Glycosaminoglycan Matrix and the Influence to Its Integrity and Stability." *2014 36th Annual International Conference of the IEEE Engineering in Medicine and Biology Society, EMBC 2014*, 3949–52. https://doi.org/10.1109/EMBC.2014.6944488.

Borel, Michele, Philippe Pastoureau, Janine Papon, Jean Claude Madelmont, Nicole Moins, Jea Maublant, and Elisabeth Miot-Noirault. 2009. "Longitudinal Profiling of Articular Cartilage Degradation in Osteoarthritis by High-Resolution Magic Angle Spinning 1H NMR Spectroscopy: Experimental Study in the Meniscectomized Guinea Pig Model." *Journal of Proteome Research* 8 (5): 2594–2600. https://doi.org/10.1021/pr8009963.

Callaghan, P T, S Godefroy, and B N Ryland. 2003. "Use of the Second Dimension in PGSE

NMR Studies of Porous Media." *Magnetic Resonance Imaging* 21 (3-4): 243-248.

https://doi.org/10.1016/S0730-725X(03)00131-0.

Comstock, J. P., and S. Udenfriend. 1970. "Effect of Lactate on Collagen Proline Hydroxylase

Activity in Cultured L-929 Fibroblasts." *Proceedings of the National Academy of*

Sciences of the United States of America 66 (2): 552–57.

https://doi.org/10.1073/pnas.66.2.552.

Fullerton, Gary D., and Andrés Rahal. 2007. "Collagen Structure: The Molecular Source of the

Tendon Magic Angle Effect." *Journal of Magnetic Resonance Imaging* 25 (2): 345–61.

https://doi.org/10.1002/jmri.20808.

Hunt, Thomas K., W. Bruce Conolly, Samuel B. Aronson, and Phillip Goldstein. 1978.

"Anaerobic Metabolism and Wound Healing: An Hypothesis for the Initiation and

Cessation of Collagen Synthesis in Wounds." *The American Journal of Surgery* 135 (3):

328–32. https://doi.org/10.1016/0002-9610(78)90061-2.

Koivunen-niemelä, T., M. Komu, J. Viikari, and A. Alanen. 1994. "Mri and Mrs of Human

Tendon Xanthoma at 1.5 t: An in Vivo Study." *Magma Magnetic Resonance Materials in*

Physics, Biology, and Medicine 2 (2): 121–26. https://doi.org/10.1007/BF01753068.

Kwan, Ann H., Mehdi Mobli, Paul R. Gooley, Glenn F. King, and Joel P. MacKay. 2011.

"Macromolecular NMR Spectroscopy for the Non-Spectroscopist." *FEBS Journal* 278

(5): 687–703. https://doi.org/10.1111/j.1742-4658.2011.08004.x.

Li, Jingbo, Thomas Vosegaard, and Zheng Guo. 2017. "Applications of Nuclear Magnetic

Resonance in Lipid Analyses: An Emerging Powerful Tool for Lipidomics Studies."

Progress in Lipid Research 68 (September): 37–56.

https://doi.org/10.1016/j.plipres.2017.09.003.

Ling, Wen, Ravinder R. Regatte, Mark E. Schweitzer, and Alexej Jerschow. 2008.

"Characterization of Bovine Patellar Cartilage by NMR." *NMR in Biomedicine* 21 (3): 289–95. https://doi.org/10.1002/nbm.1193.

Loss, Sandra, Kühn, Till. 2005. "Basic 1D and 2D Experiments Introduction to 1- and 2-Dimensional NMR Spectroscopy." *Bruker*, 190.

Lowe, I. J. 1959. Free induction decays of rotating solids. *Physical Review Letters 2: 2*285–287. doi:10.1103/PhysRevLett.2.285.

Monteilhet, L, J Mitchell, and P J Mcdonald. 2006. "Observation of Exchange of Micropore Water in Cement Pastes by Two-Dimensional T 2 - T 2 Nuclear Magnetic Resonance Relaxometry," 1–9. https://doi.org/10.1103/PhysRevE.74.061404.

Mucci, A., L. Schenetti, and N. Volpi. 2000. "1H and 13C Nuclear Magnetic Resonance Identification and Characterization of Components of Chondroitin Sulfates of Various Origin." *Carbohydrate Polymers* 41 (1): 37–45. https://doi.org/10.1016/S0144-8617(99)00075-2.

Peto, S., P. Gillis, and V. P. Henri. 1990. "Structure and Dynamics of Water in Tendon from NMR Relaxation Measurements." *Biophysical Journal* 57 (1): 71–84. https://doi.org/10.1016/S0006-3495(90)82508-X.

S., Moestue, Sitter B., Bathen T.F., Tessem M.-B., and Gribbestad I.S. 2011. "HR MAS MR Spectroscopy in Metabolic Characterization of Cancer." *Current Topics in Medicinal Chemistry* 11 (1): 2–26. http://ovidsp.ovid.com/ovidweb.cgi?T=JS&PAGE=reference&D=emed10&NEWS=N&AN=2010674892.

Schiller, J., L. Naji, D. Huster, J. Kaufmann, and K. Arnold. 2001. "1H and 13C HR-MAS NMR

Investigations on Native and Enzymatically Digested Bovine Nasal Cartilage." *Magma (New York, N.Y.)* 13 (1): 19–27. https://doi.org/10.1007/bf02668647.

Schiller, Jürgen, Daniel Huster, Beate Fuchs, Lama Naji, Jörn Kaufmann, and Klaus Arnold. 2004. "Evaluation of Cartilage Composition and Degradation by High-Resolution Magic-Angle Spinning Nuclear Magnetic Resonance." *Methods in Molecular Medicine* 101 (1): 267–85. https://doi.org/10.1385/1-59259-821-8:267.

Scott, Alex, Johannes Zwerver, Navi Grewal, Agnetha De Sa, Thuraya Alktebi, David J. Granville, and David A. Hart. 2015. "Lipids, Adiposity and Tendinopathy: Is There a Mechanistic Link? Critical Review." *British Journal of Sports Medicine* 49 (15): 984–86. https://doi.org/10.1136/bjsports-2014-093989.

Screen, Hazel R. C., David E. Berk, Karl E. Kadler, Francesco Ramirez, and Marian F. Young. 2015. "Tendon Functional Extracellular Matrix." *Journal of Orthopaedic Research* 33 (6): 793–99. https://doi.org/10.1002/jor.22818.

Shoulders, Matthew D., and Ronald T. Raines. 2009. "Collagen Structure and Stability." *Annual Review of Biochemistry*. NIH Public Access. https://doi.org/10.1146/annurev.biochem.77.032207.120833.

Smeets, Joey S.J., Astrid M.H. Horstman, Georges F. Vles, Pieter J. Emans, Joy P.B. Goessens, Annemie P. Gijsen, Janneau M.X. van Kranenburg, and Luc J.C. van Loon. 2019. "Protein Synthesis Rates of Muscle, Tendon, Ligament, Cartilage, and Bone Tissue in Vivo in Humans." *PLoS ONE* 14 (11): 1–17. https://doi.org/10.1371/journal.pone.0224745.

Spang, Christoph, Ludvig J. Backman, Sandrine Le Roux, Jialin Chen, and Patrik Danielson. 2017. "Glutamate Signaling through the NMDA Receptor Reduces the Expression of

Scleraxis in Plantaris Tendon Derived Cells." *BMC Musculoskeletal Disorders* 18 (1): 1–13. https://doi.org/10.1186/s12891-017-1575-4.

Thorpe, Chavaunne T., Helen L. Birch, Peter D. Clegg, and Hazel R.C. Screen. 2013. "The Role of the Non-Collagenous Matrix in Tendon Function." *International Journal of Experimental Pathology* 94 (4): 248–59. https://doi.org/10.1111/iep.12027.

Warner, Joshua. 2010. "Developments in 2D NMR Relaxometry and Its Application to Biological Tissue," (Dissertation)

Woessner, Donald E. 1996. "Brownian Motion and Its Effects in NMR Chemical Exchange and Relaxation in Liquids." *Concepts in Magnetic Resonance* 8 (6): 397–421. https://doi.org/10.1002/(SICI)1099-0534(1996)8:6<397::AID-CMR2>3.0.CO;2-U.

Yamauchi, M., R. E. London, C. Guenat, F. Hashimoto, and G. L. Mechanic. 1987. "Structure and Formation of a Stable Histidine-Based Trifunctional Cross-Link in Skin Collagen." *Journal of Biological Chemistry* 262 (24): 11428–34. https://doi.org/10.1016/s0021-9258(18)60824-5.

Yamauchi, Mitsuo, Masahiko Terajima, and Masashi Shiiba. 2019. "Lysine Hydroxylation and Cross-Linking of Collagen." In *Methods in Molecular Biology*, 1934:309–24. Humana Press Inc. https://doi.org/10.1007/978-1-4939-9055-9_19.
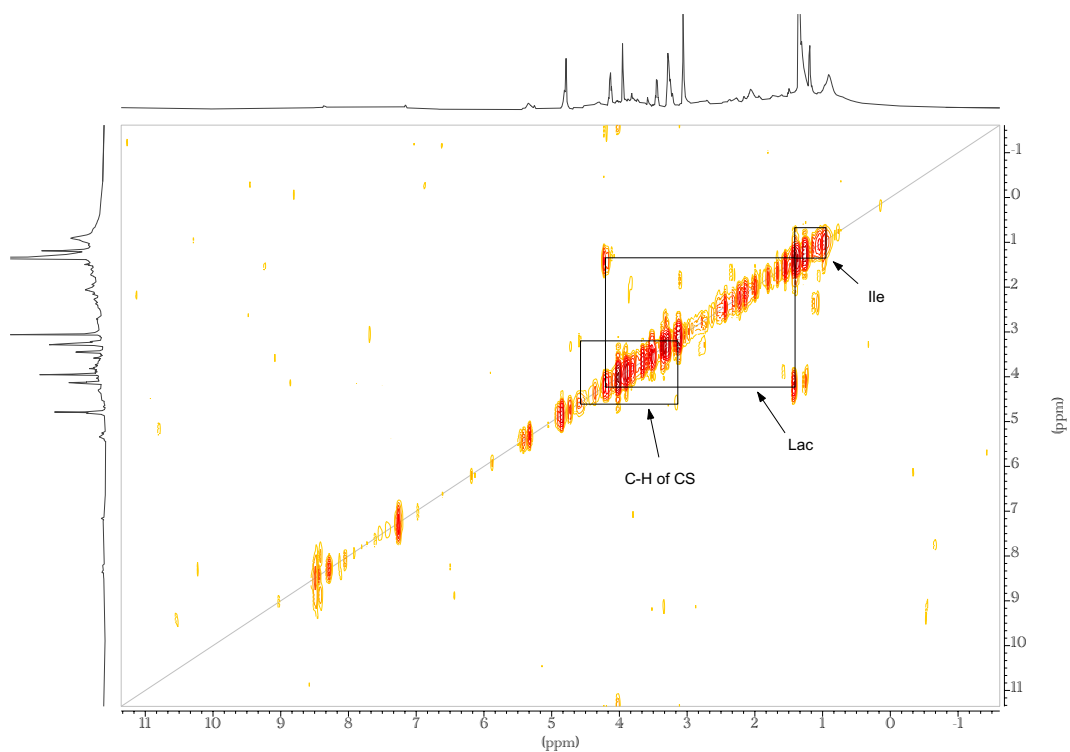
VII.   Supplemental Figures
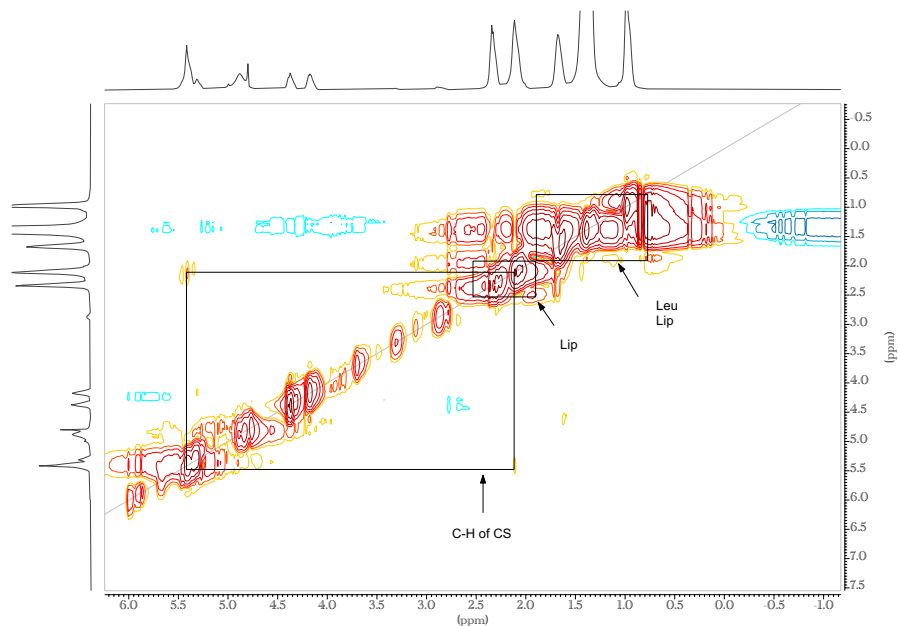
Supplementary Figure 1. 2D COSY spectrum of ovine Achilles tendon. Peaks on the diagonal represent couplings between the same proton chemical groups. Off-diagonal peaks represent coupling between chemically non-equivalent protons. Boxes represent the most significant correlations.
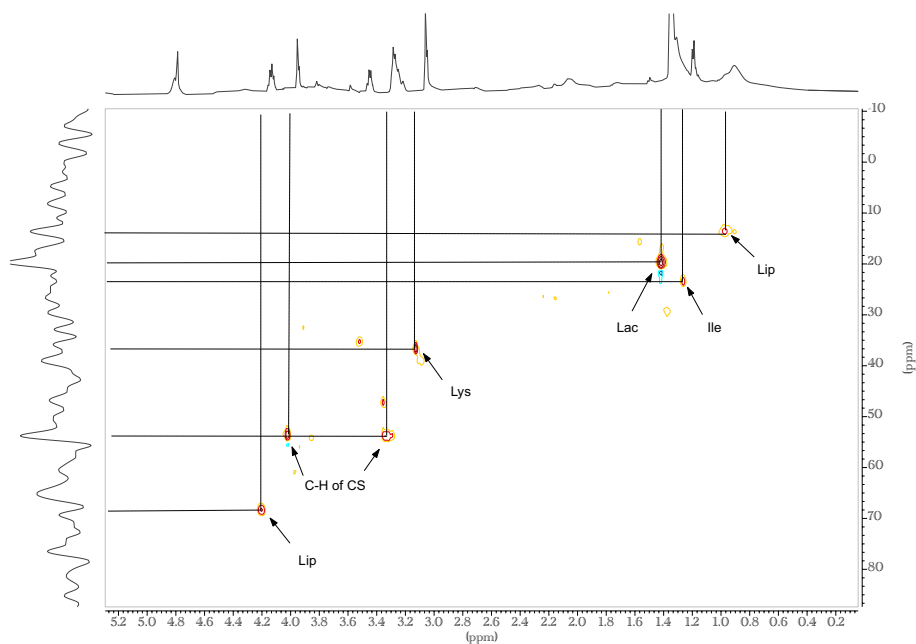
Supplementary Figure 2. 2D HSQC spectrum of rat rotator cuff tendon. Peaks represent protons coupled to their respective attached carbons.

Supplementary Figure 3. 2D COSY spectrum of rat rotator cuff tendon. Peaks on the diagonal represent couplings between the same proton chemical groups. Off-diagonal peaks represent coupling between chemically non-equivalent protons. Boxes represent the most significant correlations.